Characterisation of $J(\mathrm{O}^1\mathrm{D})$ at Cape Grim 2000–2005

S. R. Wilson

Centre for Atmospheric Chemistry, School of Chemistry, University of Wollongong, NSW, Australia

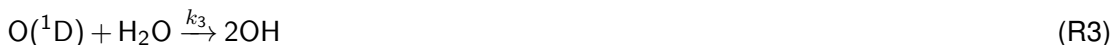Correspondence to: S. R. Wilson (swilson@uow.edu.au)

Abstract

Estimates of the rate of production of excited oxygen atoms due to the photolysis of ozone ($J(O^1D)$) have been derived from radiation measurements carried out at Cape Grim, Tasmania ($40.6°$ S, $144.7°$ E). The measurements have a total uncertainty of 15 % (1σ). These estimates agree well with model estimates of clear sky photolysis rates. Observations spanning 2000–2005 have been used to quantify the impact of season, clouds and ozone column amount. The annual cycle of $J(O^1D)$ has been investigated via monthly means. These means show an inter-annual variation (monthly standard deviation) of 9 %, but in midsummer and midwinter this reduces to 3–5 %. Variations in solar zenith angle and total column ozone explain 86 % of the observed variability in the measured photolysis rates. The impact of total column ozone, expressed as a Radiation Amplification Factor (RAF), is found to be ~ 1.53, in agreement with model estimates. This ozone dependence explains 20 % of the variation observed at medium solar zenith angles ($30–50°$). The impact of clouds results in a median reduction of 30 % in $J(O^1D)$ for the same solar zenith angle range. Including estimates of cloudiness derived from Long Wave Radiation measurements resulted in a statistically significant fit to observations but the quality of the fit did not increase significantly as measured by the adjusted R^2.

1 Introduction

It is widely recognised that the chemistry of the clean troposphere is driven by a few key oxidizing species, with a major contributor being the hydroxyl radical (OH) (Crutzen, 1974). The hydroxyl radical reacts rapidly with a wide range of compounds, including methane, CO, and hydrocarbons. The concentration of OH present in the atmosphere is always small, but because of its high reactivity it can still play a dominant role in determining the atmospheric fate of organics. It has also long been realised that changes in the amount of OH in the atmosphere could have a profound effect on global air quality and there has been a long-term effort to develop techniques to measure the key chemical species (Heard and Pilling, 2003).

2

The most direct measure is the concentration of OH itself. There are several techniques now in use for such measurements, including fluorescence, UV absorption and mass spectrometry (Heard and Pilling, 2003) although long term measurement sets are rare (Rohrer and Berresheim, 2006; Berresheim et al., 2013).

5   The primary source of OH is through the photolysis of ozone to produce $O(^1D)$ through the reactions:

$$O_3 + h\nu \xrightarrow{J(O^1D)} O(^1D) + O_2 \left(^1\Delta_g, ^3\Sigma_g^-\right) \tag{R1}$$

$$O(^1D) + M \xrightarrow{k_2} O(^3P) \tag{R2}$$

$$O(^1D) + H_2O \xrightarrow{k_3} 2OH \tag{R3}$$

10   The fraction of $O(^1D)$ reacting with water (and hence producing OH) (Q) is given by:

$$Q = k_3[H_2O]/(k_3[H_2O] + \sum_i k_i[M_i]) \tag{1}$$

Here the summation is over the collision partners M_i, primarily O_2 and N_2. Q depends on the amount of water vapour, but typically around 10 % of $O(^1D)$ produced reacts to form OH ($Q \approx 0.1$). This can be calculated provided atmospheric pressure and the water vapour
15   concentration is known, since the rate constants have been measured (Sander et al., 2006).

The rate of ozone photolysis in Reaction (R1), $J(O^1D)$, can be described by:

$$J(O^1D) = \int \sigma(\lambda, T)\phi(\lambda, T)F(\lambda)d\lambda \tag{2}$$

which is the wavelength integration of $\sigma(\lambda, T)$, the (temperature dependent) absorption cross-section of ozone, $\phi(\lambda, T)$, the quantum yield of $O(^1D)$ production, and $F(\lambda)$, the
20   "spectral actinic flux density", which is the spherically integrated spectral radiance. There are a number of measurements of $J(O^1D)$ via chemical actinometers (Hofzumahaus et al., 2004), although due to their nature they are difficult to deploy for long periods of time, making either filter radiometers or spectral radiometers an attractive alternative (Bohn et al., 2008).

3

1.1 Techniques for the measurement of actinic flux density (F)

There are a range of radiometric techniques used for the determination of actinic flux, and the strengths of various detectors has been assessed by a field comparison experiment (Bohn et al., 2008). All these techniques relied on calibrations using reference light sources.

1.1.1 Estimating actinic flux density from irradiance measurements

The ideal viewing geometry for the determination of $F(\lambda)$ detects photons from all directions equally (all 4π steradian). For locations not over reflective surfaces like snow the upwelling radiation is relatively small, and so most measurements of $F(\lambda)$ are made viewing downwelling radiation only (e.g., Junkermann et al., 1989). In the following section all terms have a wavelength dependence. The (λ) has been omitted in equations 3 - 6. The term "spectral" should also be used for the quantities listed in these equations. Both omissions have been made for clarity.

Most quantitative UV observations measure global irradiance (E) (the radiative power striking a horizontal plane), and so there have been a number of attempts to convert global irradiance into actinic flux (Kazadzis et al., 2004; Kylling et al., 2003; McKenzie et al., 2002; Schallhart et al., 2004; Webb et al., 2002).

If it is assumed that there is no upwelling radiation (surface albedo $= 0$), the actinic flux is given by

$$F = F_0 + F_\downarrow \tag{3}$$

where F_0 is the direct actinic flux and $F_\downarrow$ is the diffuse flux. Similarly, the global irradiance (E) is given by

$$E = \mu E_0 + E_\downarrow \tag{4}$$

where E_0 is now the direct beam irradiance, $\mu = \cos\theta$ where θ is the solar zenith angle and $E_\downarrow$ is the diffuse irradiance. As $E_0 = F_0$, it is now possible to simply write

$$F = \alpha E_\downarrow + E_0 = \alpha(E - \mu E_0) + E_0 \tag{5}$$

4

where α is the ratio of the diffuse actinic flux to diffuse irradiance. If the diffuse irradiance is not measured, this can be rearranged into the following relationship suggested by Kazadzis et al. (2004).

$$\frac{F}{E} = \alpha + (1 - \alpha\mu)\frac{E_0}{E} \qquad (6)$$

The ratio α needs to be determined at the wavelengths relevant for the $O(^1D)$ photolysis (McKenzie et al., 2002; Webb et al., 2002), and this will be discussed in Section 3.1.

Estimating the ratio of the direct beam to global irradiance (E_0/E) has been more difficult. Schallhart et al. (2004) have therefore used a semi-empirical method which parameterized the relationship (F/E) based on the ratio of observed irradiance to clear sky irradiance, where the clear sky irradiance is calculated. Using data from four locations they found their results gave better agreement between measured and calculated F (7%, 2σ) than that reported using Eq. (6) and no knowledge of the direct to global irradiance ratio (Kylling et al., 2003; Webb et al., 2002). Using global irradiance measurements of with direct irradiance every 10 nm, Kazadzis et al. (2004) estimate an overall uncertainty in F of around 10% (1σ).

1.1.2 Strategies for spectral measurements

Three types of systems have been used in the past to determine $J(O^1D)$; a filter radiometer, a scanning spectrometer, or a diode array/CCD detector equipped spectrometer system (Bohn et al., 2008; Hofzumahaus et al., 2004). Each approach has limitations. The filter radiometer measures at a fixed wavelength range, which needs then to be calibrated using the actual atmospheric ozone column and solar zenith angle factors (Bohn et al., 2004). The scanning spectrometer takes time to scan through the spectrum, rather than measuring at a fixed time, leading to measures that are "time-smeared" rather than "time-averaged". For the production of a short-lived species like $O(^1D)$ this can lead to difficulties in comparing with other measurements. Finally, the diode array/CCD system needs to have well

5

characterized stray-light corrections applied (Bohn et al., 2008; Hofzumahaus et al., 2004; Edwards and Monks, 2003).

1.2 Estimates of $J(O^1D)$ at Cape Grim

The Cape Grim Baseline Air Pollution Station ("Cape Grim"), (40°40′56″ S, 144°41′18″ E)
5 is a site near the northwest tip of Tasmania that experiences periods of clean maritime air from the southern ocean. During two intensive measurement campaigns SOAPEX-1 (1995) (Monks et al., 1998) and SOAPEX-2 (1999) (Creasey et al., 2003) filter radiometers have been deployed to measure $J(O^1D)$. During SOAPEX-2 the OH concentration was also measured. The measurements during the second campaign clearly demonstrated a sim-
10 ple link between $O(^1D)$ production and OH concentrations in clean atmosphere conditions (Creasey et al., 2003).

As part of the Cape Grim measurement program spectral UV-B irradiance (both global and diffuse) has been measured routinely. The purpose of this work is to use the spectral UV-B measurements to estimate $J(O^1D)$ for the period 2000–2005, to assess estimates of
15 the photolysis rates and to then develop a climatology. In particular, the impact of clouds and ozone will be assessed.

2 Experimental Setup

All UV-B irradiance measurements reported here have been made in the radiation enclosure at the Cape Grim Baseline Air Pollution Station. This is located some 300 m north of
20 the main building (Cainey et al., 2007). The location avoids the shadow of the telecommunication tower that is situated just to the north of the main building. The experimental details of the UV-B measurements and in-situ calibration technique have been reported elsewhere (Wilson and Forgan, 1995; Wilson, 2006, 2007). In brief, the system alternately measures global and diffuse irradiance with a scanning double monochromator (Optronics Labora-
25 tories OL752) known as SRAD. Diffuse irradiance is measured by the global diffuser with a small shading disk mounted on the elevation arm of a sun tracker (Wilson, 2006). The

6

spectral scans are spaced at 5–10 min intervals, depending upon the time of day. The instrument is calibrated at 342 nm using well characterized sunphotometer measurements of direct beam irradiance, and the other wavelengths calibrated using the Ratio-Langley technique (Wilson and Forgan, 1995). All this is referenced to a top of the atmosphere spectrum (Chance and Kurucz, 2010) which serves as the primary calibration of both wavelength and intensity. The optical input for the system was modified in October 1999, resulting in higher optical throughput (and hence better signal/noise ratios) and a diffuser with a better cosine response. The focus of this work is therefore on the period after the change in diffuser.

It is worth noting that the cosine error of the diffuser is determined from the solar zenith angle dependence of the ratio of the SRAD–derived direct beam irradiance to the sunphotometer. A correction for this variation can then be applied during the calibration.

The resulting database of measurements includes alternating estimates of global and diffuse irradiance at each wavelength and time. The determination of the components of the irradiance at a single time is based on interpolation of the diffuse/global measurements before and after the global/diffuse measurement in question (Wilson and Forgan, 1995), and so the derived signals are an approximation of the value for the 10–20 min period around the nominal measurement time.

The input diffuser was constructed from PTFE but was not temperature controlled. The phase change reported for this material at around 292 K (Ylianttila and Schreder, 2005) is therefore a source of uncertainty in these measurements. This will also impact the calibration, so that this effect will be at least partially captured in the variability of the calibrations.

3 Methodology

3.1 Derivation of $J(\mathrm{O^1D})$ production from UV-B measurements

As the Cape Grim UV data set includes both the diffuse and global irradiance, Eq. (5) can be used, as the direct beam irradiance can be derived from the difference between the global and diffuse component (see Eq. 4). This leaves the determination of the ratio α. For

the wavelength region of interest (300–330 nm), a value of 2.0 could be used, which is the value appropriate for isotropic radiation (McKenzie et al., 2002) and clear skies. In cloudy conditions α decreases. The calculations have been carried out using both the clear sky estimate of α and a value of 1.73, typical of cloudy conditions (Kylling et al., 2003). For the analysis here the values using the lower value for α have been used unless otherwise noted.

For the ozone absorption cross section ($\sigma\,(\lambda, T)$, Eq. 2) the measurements of Malicet et al. (1995) at 22 °C have been used, in conjunction with the temperature dependent O^1D quantum yield (Sander et al., 2006), derived using the hourly average air temperature measured at Cape Grim (as part of the meteorology program) (Cainey et al., 2007).

The UV-B measurements span the region 298–335 nm, and this can lead to an underestimate of the photolysis rate as the product $\sigma.\phi.F$ (see Eq. 2) can be non-zero outside this wavelength range. A study by Jäkel et al. (2006) found that cut-offs below 298 nm did not perturb the estimate of $J(O^1D)$ by more than 5 %, with the maximum error at times of low column ozone and high sun. Test measurements using spectra measuring out to 340 nm found that including the region between 335–340 nm altered $J(O^1D)$ by less than 1 %. There is no recommended quantum yield for O^1D above 340 nm (Sander et al., 2006). The estimates presented here will therefore be biased low by the limited wavelength coverage by typically less than 5 %.

The uncertainty in these derived $J(O^1D)$ values have been estimated, with details given in the supplementary information. In brief, the irradiance measures are estimated to have a calibration uncertainty (1σ) of 5.5 %. The combined uncertainty of all terms contributing to the calculation of $J(O^1D)$ is found to be 15 % (1σ). This uncertainty estimate does not include the impact of model assumptions including the assumption of isotropic diffuse irradiance.

3.2 Modeling $J(O^1D)$

In the analysis of data the model TUV version 5.0 has been used (Madronich and Flocke, 1997). One of the changes in this version of the model is the use of the same solar spectrum

8

(Chance and Kurucz, 2010) as that used for the calibration of SRAD. The calculations have been run at a range of solar zenith angles using an aerosol optical depth of 0.05 at 550 nm, a value typical of conditions at Cape Grim (Wilson and Forgan, 2002). The ozone column amount used is derived from satellite measurements (TOMS) (http://disc.sci.gsfc.nasa.gov/

5 acdisc/TOMS). Because the model uses the same spectral data (top of the atmosphere spectrum, ozone cross section, quantum yield) and only considers clear sky conditions, the agreement between measurements and model could approach the uncertainty in the calibration, which is estimated to be around 6 % (Supplementary material), although this does not include an estimate for the uncertainty in the ozone column or any estimate of the

10 uncertainty in the model.

4 Results and discussion

4.1 Comparison of measured $J(O^1D)$ with model estimates

The measurements can be compared with the clear sky calculations performed using TUV 5.0, where the experimentally derived values have been estimated using both a clear sky

15 and cloudy estimate of α. The results of this are shown in Fig. 1. It can be seen that for the data from both February 2000 (low column ozone) and October 2003 (high column ozone) there is good agreement between model and measurement (average deviation 2 %) if the appropriate value (clear sky) of α is used. Differences at high sun are around 3 %. Several days exist where the irradiance appears to vary smoothly but with differences of up to 10 %

20 at solar noon. This could be due in part to the limited measurement range (Sect. 3.2), a calibration issue that occurs at these solar zenith angles, aerosol, ozone column estimate errors or due to clouds. The aerosol optical depth does not appear large (based on the sun photometer) and the ozone retrieved using the midday calibration are not substantially different from the satellite. The smooth change in $J(O^1D)$ implies no clouds near the sun,

25 but there can be clouds well away from the sun that is altering the observed photolysis rate. Without a measure of the cloud field it is hard to distinguish between these possibilities.

9

4.2 Annual cycle in $J(O^1D)$

The data collected for the period 2000–2005 are shown in Fig. 2. The dataset comprises over 108 000 measurements. The gaps in the dataset represent times when the equipment failed.

5   The annual cycle is the dominant feature in this plot. To quantify this, monthly mean values have been calculated by sorting all data from a month into 24 hourly bins, and from these bins producing an average daily cycle for each month. It is assumed that if no measurement is made in one of the 24 hourly bins during the month that the average is zero. The average of the 24 hourly averages is then calculated for each month in the 6 years.
10   This method has been used to limit the impact of possible biases from collecting spectra at varying time intervals.

Despite the variability seen in the individual measurements (see Fig. 2), the monthly averages are relatively stable (Fig. 3, top panel). The lower panel of Fig. 3 shows that for mid-summer and mid-winter the interannual variability in the monthly averages is 3–
15   5 %, with the increases in-between presumably driven by the the observed annual cycle. That is, during Spring and Autumn it matters more when in the month the measurements have been made. Changes in ozone column amount could be a contributing factor. Using the coincident satellite ozone data shows a maximum in ozone variability in mid-winter, suggesting that ozone is not the main driving force. The resultant average monthly $J(O^1D)$
20   for Cape Grim is also presented in Table 1 along with the standard deviations.

Measurements of $J(O^1D)$ have been reported for 2002 – 2006 in the eastern Mediterranean (Gerasopoulus et al., 2012). The interannual variability in the monthly mean maximum clear sky irradiance is of the order of 7 – 8 %. This is comparable to the monthly relative standard deviation in all measurements at Cape Grim (9.2 %). The two locations
25   are very different, both in terms of aerosol loadings and cloudiness, so the similarity is not expected.

Earlier measurements of interannual variability of UV-B have been reported for Ushuaia in Argentina (Frederick et al., 2001). For global irradiance at 305 nm they found an interannual

10

variability (standard deviation) of around 25 %. The variability in global irradiance could be expected to be bigger than that for $J(O^1D)$ with the different dependence on the angle of incidence of radiation. The mean of the monthly relative standard deviation (9.2 %) is indeed slightly lower than that observed for global UV-B irradiance (10.8 %) as determined from the

5 Cape Grim data. However, both are significantly less than reported from Argentina. This is presumably a reflection of the difference in climate or ozone.

To investigate any trend in the data both monthly trends for each month and trends as a function of season have been calculated. The most significant linear trend is in summer (December–February) (-1.7 ± 1.1 (std. dev.) % year^{-1}), but this is not significant at the 90 %

10 level. Satellite estimates of changes in irradiance at 305 nm due to stratospheric ozone and clouds at this latitude are 0.3–0.4 % year^{-1} (averaged over 1979–2008) (Herman, 2010). For the shorter period measured here it is not possible to detect changes of that magnitude, and local effects on cloudiness could determine the magnitude (and sign) of the observed trend.

4.3 Ozone column dependence

15 The dependence of $J(O^1D)$ on solar zenith angle has been determined by sorting all data into 5° bins, and the results are summarized in Fig. 4. For this plot, zenith angles up to 82.5° have been included. All measurements have been adjusted to 1 a.u. (correction for the annual variation in the earth-sun distance; Iqbal, 1983). A few measurements made at solar zenith angles below 17.5° have been excluded as they represent a brief period in

20 mid-summer. Included in the plot are $J(O^1D)$ estimates calculated using the TUV model for cloud free conditions and an aerosol optical depth of 0.05. Calculations for two ozone column amounts are shown, 250 and 350 DU, which are typical seasonal maximum and minimum values observed in this location as derived from satellite measurements (TOMS).

A significant fraction of the variability can be due to the differences in the ozone column

25 during the year. To characterize the dependence, functions of the following form were fitted

11

to the measured $J(O^1D)$:

$$J(O^1D) = \left(\sum_i A_i \exp(-B_i/\cos\theta) \right) \cdot \left(O_3^{sat}/300 \right)^{-RAF} \tag{7}$$

where θ is the solar zenith angle, O_3^{sat} is the total ozone column retrieved from satellite for the measurement day, and A_i, B_i and RAF are fitted. RAF is the Radiation Amplification

5 Factor to be determined (Micheletti et al., 2003). The results for the fit to the entire dataset using either one or two exponential terms ($i = 1$ or 2) are shown in Table 2 and for one exponential term in Fig. 4. Using two exponentials produces a slightly better fit, and both fits produce an RAF estimate in reasonable agreement with calculations of 1.4–1.5 (McKenzie et al., 2011).

10 Using this derived ozone RAF the dataset was normalized to both 300 DU and 1 a.u. as shown in Fig. 5. Given the large difference between the median and average values for the bins, a second fit was performed to the median of the binned values of Fig. 5, and the fits are also included in Table 2. For reference, the fits with two exponential terms, using all data and the medians is included in Fig. 5. It should be noted that the increase in R^2 is due to

15 the change in the nature of the data being fitted.

The removal of the variation due to changes in stratospheric ozone, as described by the satellite ozone measurements, reduces the interquartile variability by up to 20 % as shown in Fig. 6. The effect on high sun (small solar zenith angle) measurements is smaller, as this is only collected in mid-summer and so the ozone variability is small. At larger solar zenith

20 angles ($> 50°$) the percentage reduction diminishes also, presumably because, as the absolute intensity decreases, other effects, including the impact of measurement uncertainty, become larger.

4.4 Cloud impact

Clouds can both reduce and enhance solar radiation at the ground level. Figure 5 shows

25 that the 99th percentile value is close to the clear-sky calculated value at solar zenith angles

less than 50°. This suggests that the measurements are dominated by cloud attenuation, with little evidence of an enhancement of radiation due to clouds, (Calbó et al., 2005). At solar zenith angles greater than 65°, a larger fraction of observations exceed the clear sky calculation. There is no data to support more broken cloud conditions which could lead to enhancement. It seems more likely that this is due to unidentified detector cosine errors, limitations in the interpolation used to determine the direct beam and diffuse irradiance, or errors in the model.

To assess the overall impact of clouds, the ratio of the median value to the calculated clear – sky value was determined (Fig. 7). This shows that for solar zenith angles less than 70° the median is approximately 70 % of the calculated clear sky value. From 20–70° the calculated impact of clouds on $J(O^1D)$ increases by 15 %, a trend also predicted in models of the cloud impact on UV irradiance (Lindfors and Arola, 2008; Mateos et al., 2014).

The results for solar zenith angles greater than 70° show that clouds have a diminishing impact as the sun approaches the horizon. A similar observation has been made in both calculations and observations (Mateos et al., 2014). However, both measurement uncertainties (due to smaller signals and variations in detector angular response) and modelling limitations may well be playing a significant role. The enhancement in inter-quartile range, also shown in Fig. 7, could also be due to measurement uncertainty.

Attempts to capture the cloud variability through independent observations have not been very successful. Measures such as visual observations and automatic sky cameras have not been implemented at Cape Grim. While sunphotometers make measurements during this period, they do not make measurements of cloud optical depth as has been used elsewhere (Anton et al., 2012). Longwave downward radiation (LDR) measurements have been used to estimate cloudiness (Marty and Philipona, 2000; Dürr and Philipona, 2004). The attraction of this measure is that LDR is relatively insensitive to the solar position, and so should be independent of the other factors influencing $J(O^1D)$. An attempt at using LDR has been made using half-hourly long-wave radiation averaged values measured at Cape Grim (Wilson and Shinkfield, 2007) to derive the Clear-Sky Index (Marty and Philipona, 2000). In this case it was possible to produce a fit extending Eq. (8) with an additional

term (Clear-Sky Index)$^{\alpha}$, where α is a fitted parameter. Fitting the entire dataset where LDR values were available returned a significant value for the exponent (-0.19 ± 0.01). However, the fit did not improve significantly, as measured by the adjusted R^2 (increases of ~ 0.0005), implying that this is not a useful approach. This could be due to the insensitivity

5 of long-wave radiation measures to higher-level clouds (Schade et al., 2009; Boers et al., 2010). However, cloud bases are often low at Cape Grim (800 - 1000 m), as observed by LIDAR measurements, (Young, 2007) and so LDR should be a reasonable measure. It is more likely that the features of clouds that cause changes in the observed LDR are not simply related to those features which result in a significant reduction (or enhancement) of

10 $J(O^1D)$.

A dependence of $J(O^1D)$ on aerosols has been identified in measurements in the eastern Mediterranean (Gerasopoulus et al., 2012), which could in principle be part of the variation identified here as a cloud impact. However, the low aerosol optical depth (mean of 0.07 at 500 nm compared with 0.23 in the Mediterranean (Gerasopoulus et al., 2011)) makes this

15 a small effect, especially when compared to the very common cloud cover at Cape Grim.

4.5 Wider relevance of the observations

The atmospheric composition at Cape Grim is dependent on wind direction and clean or "baseline" conditions are defined by standard measures (Downey, 2007). The impact on atmospheric chemistry of the photolysis measured here will depend on whether the local

20 atmosphere is clean or polluted. However, an analysis of the data presented here filtered for only those measurements collected under "baseline" conditions gives results not statistically different from those observed for the entire dataset. As the baseline selection process eliminates a significant fraction of the data, the variability does increase.

Another important question is how reliably the climatology measured here is represen-

25 tative of a larger region. Cape Grim, sitting on the coast, could have a cloud environment different to locations out to sea and inland. A study of the global irradiance at a number of locations concluded that Cape Grim experienced cloud conditions similar to the southern ocean in this area (Bishop et al., 1997). While the station is some 90 m above sea

level, the observations remain well below the cloud base height of 800 – 100 m (Young, 2007). A study of rainfall has shown that while rainfall varies when moving inland it is reasonably constant along the coast (Jasper and Downey, 1991). The ISCCP dataset (http://isccp.giss.nasa.gov/index.html) shows that cloud amount at this latitude band over the oceans is 80–90 %, with little dependence on longitude and without an obvious trend over the period 1984–2008. Therefore, the cloud impacts observed at Cape Grim should be representative of the marine environment at these latitudes.

Modelling studies (Liu et al., 2006) calculated that the impact of clouds on $J(O^1D)$ is around -8 % averaged throughout the troposphere, but that ground level impacts are larger, of the order of -20 %. The data presented here shows an impact of clouds on $J(O^1D)$ somewhat larger than the calculation. The reduction is less than that often observed for global UV irradiance at 50 % cloud cover (Calbó et al., 2005), underlining the relative insensitivity of actinic flux density to clouds. This is a result of the relative importance of diffuse radiation to the photolysis rate, and the limited impact of clouds on total diffuse irradiance (Blumthaler et al., 1994).

The results of this study permit the prediction of $J(O^1D)$ in the current climate. The impact of stratospheric ozone recovery should be well described by our current understanding. However, it would be useful to estimate the likely impact of future changes in cloud properties on $J(O^1D)$. With the reasonable agreement between models and observations seen at Cape Grim there can be some confidence in their predictions. For the maritime environment investigated here the overall impact of clouds is relatively small (-30 %) given the 80–90 % cloud cover. Any future climate changes would need to change the frequency of clouds significantly to alter $J(O^1D)$ greatly. Other changes, such as a change in cloud optical depth may be more significant. Verifying any such changes in $J(O^1D)$ will require ongoing observations.

5 Conclusions

Six years of estimates of $J(O^1D)$ are presented for a clean Southern Hemisphere marine site. The impact of solar zenith angle and total column ozone can be clearly seen and quantified and the stratospheric ozone dependence is in good agreement with radiation model
[5] estimates. The impact of clouds can also be characterized, with bounds on the impact of clouds determined as a function of solar zenith angle. However, attempts at modelling the impact of clouds using independent radiation measurements (Longwave Downward Radiation) produced fits that did not significantly improve the quality of the model. So while the impact of clouds can be quantified, a good proxy for this has proven elusive.

[15] References

Antón, M., Alados-Arboledas, L., Guerrero-Rascado, J. L., Costa, M. J., C Chiu, J., and Olmo, F. J.: Experimental and modeled UV erythemal irradiance under overcast conditions: the role of cloud optical depth, Atmos. Chem. Phys., 12, 11723–11732, doi:10.5194/acp-12-11723-2012, 2012.

Berresheim, H., McGrath, J., Adam, M., Mauldin III, R. L., Bohn, B. and Rohrer, F.:Seasonal mea-
[20] surements of OH, NO_x, and $J(O^1D)$ at Mace Head, Ireland,Geophys. Res. Lett., 40(8), 1659–1663,doi:10.1002/grl.50345,2013.

Bishop, J. K. B., Rossow, W. B., and Dutton, E. G.: Surface solar irradiance from the International Satellite Cloud Climatology Project 1983–1991, J. Geophys. Res., 102, 6883–6910, doi:10.1029/96jd03865, 1997.

[25] Blumthaler, M., Ambach, W., and Salzgeber, M.: Effects of cloudiness on global and diffuse UV irradiance in a high-mountain area, Theor. Appl. Climatol., 50, 23–30, 1994.

Boers, R., de Haij, M. J., Wauben, W. M. F., Baltink, H. K., van Ulft, L. H., Savenije, M., and Long, C. N.: Optimized fractional cloudiness determination from five ground-based remote sensing techniques, J. Geophys. Res., 115, D24116, doi:10.1029/2010jd014661, 2010.

Bohn, B., Kraus, A., Muller, M., and Hofzumahaus, A.: Measurement of atmospheric $O_3 \rightarrow O(^1D)$ photolysis frequencies using filterradiometry, J. Geophys. Res., 109, D10S90, doi:10.1029/2003JD004319, 2004.

Bohn, B., Corlett, G. K., Gillmann, M., Sanghavi, S., Stange, G., Tensing, E., Vrekoussis, M., Bloss, W. J., Clapp, L. J., Kortner, M., Dorn, H.-P., Monks, P. S., Platt, U., Plass-Dülmer, C., Mihalopoulos, N., Heard, D. E., Clemitshaw, K. C., Meixner, F. X., Prevot, A. S. H., and Schmitt, R.: Photolysis frequency measurement techniques: results of a comparison within the ACCENT project, Atmos. Chem. Phys., 8, 5373–5391, doi:10.5194/acp-8-5373-2008, 2008.

Cainey, J., Derek, N., and Krummel, P. (Eds.): Baseline Atmospheric Program 2005–2006, Australian Bureau of Meteorology and CSIRO Marine and Atmospheric Research, Melbourne, 2007.

Calbó, J., Pagès, D., and González, J. A.: Empirical studies of cloud effects on UV radiation: a review, Rev. Geophys., 43, RG2002, doi:10.1029/2004rg000155, 2005.

Chance, K. and Kurucz, R. L.: An improved high-resolution solar reference spectrum for earth's atmosphere measurements in the ultraviolet, visible, and near infrared, J. Quant. Spectrosc. Ra., 111, 1289–1295, doi:10.1016/j.jqsrt.2010.01.036, 2010.

Creasey, D. J., Evans, G. E., Heard, D. E., and Lee, J. D.: Measurements of OH and HO_2 concentrations in the Southern Ocean marine boundary layer, J. Geophys. Res., 108, 4475, doi:10.1029/2002JD003206, 2003.

Crutzen, P. J.: Photochemical reactions initiated by and influencing ozone in unpolluted tropospheric air, Tellus, 26, 47–57, 1974.

Downey, A.: Meteorology/Climatology 2005–2006, in: Baseline Atmospheric Program 2005–2006, edited by: Cainey, J., Derek, N., and Krummel, P., Australian Bureau of Meteorology and CSIRO Marine and Atmospheric Research, Melbourne, 39–45, 2007.

Dürr, B. and Philipona, R.: Automatic cloud amount detection by surface longwave downward radiation measurements, J. Geophys. Res., 109, D05201, doi:10.1029/2003JD004182, 2004.

Edwards, G. D. and Monks, P. S.: Performance of a single-monochromator diode array spectroradiometer for the determination of actinic flux and atmospheric photolysis frequencies, J. Geophys. Res., 108, 8546, doi:10.1029/2002JD002844, 2003.

17

Forgan, B. W.: Sunphotometer Calibration by the Ratio-Langley Method, in: Baseline Atmospheric Program 1986, edited by: Forgan, B. W. and Fraser, P. J., 22–26, Bureau of Meteorology and CSIRO Division of Atmospheric Research, Melbourne, 1988.

Frederick, J. E., Manner, V. W., and Booth, C. R.: Interannual variability in solar ultraviolet irradiance over decadal time scales at latitude 55 deg South, Photoch. Photobio. Sci., 74, 771–779, 2001.

Gerasopoulos, E., Amiridis, V., Kazadzis, S., Kokkalis, P., Eleftheratos, K., Andreae, M. O., Andreae, T. W., El-Askary, H. and Zerefos, C. S.: Three-year ground based measurements of aerosol optical depth over the eastern mediterranean: the urban environment of Athens, Atmos. Chem. Phys., 11(5):2145–2159, doi:10.5194/acp-11-2145-2011, 2011.

Gerasopoulos, E., Kazadzis, S., Vrekoussis, M., Kouvarakis, G., Liakakou, E., Kouremeti, N., Giannadaki, D., Kanakidou, M., Bohn, B., and Mihalopoulos, N.: Factors affecting O_3 and NO_2 photolysis frequencies measured in the eastern mediterranean during the five-year period 2002–2006, J. Geophys. Res., 117, D22305, doi:10.1029/2012JD017622, 2012.

Heard, D. E. and Pilling, M. J.: Measurement of OH and HO_2 in the troposphere, Chem. Rev., 103, 5163–5198, 2003.

Herman, J. R.: Use of an improved radiation amplification factor to estimate the effect of total ozone changes on action spectrum weighted irradiances and an instrument response function, J. Geophys. Res., 115, D23119, doi:10.1029/2010jd014317, 2010.

Hofzumahaus, A., Lefer, B. L., Monks, P. S., Hall, S. R., Kylling, A., Mayer, B., Shetter, R. E., Junkermann, W., Bais, A., Calvert, J. G., Cantrell, C. A., Madronich, S., Edwards, G. D., Kraus, A., Muller, M., Bohn, B., Schmitt, R., Johnston, P., McKenzie, R., Frost, G. J., Griffioen, E., Krol, M., Martin, T., Pfister, G., Roth, E. P., Ruggaber, A., Swartz, W. H., Lloyd, S. A., and Van Weele, M.: Photolysis frequency of O_3 to $O(^1D)$: measurements and modeling during the International Photolysis Frequency Measurement and Modeling Intercomparison (IPMMI), J. Geophys. Res., 109, D08S90, doi:10.1029/2003JD004333, 2004.

Iqbal, M.: An Introduction to Solar Radiation, Academic Press, Toronto, 1983.

Jäkel, E., Wendisch, M., and Lefer, B.: Parameterization of ozone photolysis frequency in the lower troposphere using data from photodiode array detector spectrometers, J. Atmos. Chem., 54, 67–87, doi:10.1007/s10874-006-9014-1, 2006.

Jasper, J. D. and Downey, A. H.: Towards a Cape Grim Climatology, in: Baseline Atmospheric Program 1989, edited by: Wilson, S. R. and Gras, J. L., Bureau of Meteorology and the CSIRO Division of Atmospheric Research, Melbourne, 38–46, 1991.

Junkermann, W., Platt, U., and Volz-Thomas, A.: A photoelectric detector for the measurement of photolysis frequencies of ozone and other atmospheric molecules, J. Atmos. Chem., 8, 203–227, 1989.

Kazadzis, S., Topaloglou, C., Bais, A. F., Blumthaler, M., Balis, D., Kazantzidis, A., and Schallhart, B.: Actinic flux and O^1D photolysis frequencies retrieved from spectral measurements of irradiance at Thessaloniki, Greece, Atmos. Chem. Phys., 4, 2215–2226, doi:10.5194/acp-4-2215-2004, 2004.

Kylling, A., Webb, A. R., Bais, A., Blumthaler, M., Schmitt, R., Thiel, S., Kazantzidis, A., Kift, R., Misslbeck, M., Schallhart, B., Schreder, J., Topaloglou, C., Kazadzis, S., and Rimmer, J.: Actinic flux determination from measurements of irradiance, J. Geophys. Res., 108, 4506, doi:10.1029/2002JD003236, 2003.

Lindfors, A. and Arola, A.: On the wavelength-dependent attenuation of UV radiation by clouds, Geophys. Res. Lett., 35, L05806, doi:10.1029/2007GL032571, 2008.

Liu, H., Crawford, J. H., Pierce, R. B., Norris, P., Platnick, S. E., Chen, G., Logan, J. A., Yantosca, R. M., Evans, M. J., Kittaka, C., Feng, Y., and Tie, X.: Radiative effect of clouds on tropospheric chemistry in a global three-dimensional chemical transport model, J. Geophys. Res., 111, D20303, doi:10.1029/2005JD006403, 2006.

Madronich, S. and Flocke, S.: Theoretical Estimation of Biologically Effective UV Radiation at the Earth's Surface, in: Solar Ultraviolet Radiation-Modeling, Measurements and Effects, edited by: Zerefos, C. and Bais, A., NATO ASI Subseries 1, Vol. 52, Springer-Verlag, Berlin, 23–48, 1997.

Malicet, J., Daumont, D., Charbonnier, J., Parisse, C., Chakir, A., and Brion, J.: Ozone UV spectroscopy. 2. Absorption cross-sections and temperature dependence, J. Atmos. Chem., 21, 263–273, 1995.

Marty, C. and Philipona, R.: The clear-sky index to separate clear-sky from cloudy-sky situations in climate research, Geophys. Res. Lett., 27, 2649–2652, doi:10.1029/2000gl011743, 2000.

Mateos, D., di Sarra, A., Bilbao, J., Meloni, D., Pace, G., de Miguel, A., and Casasanta, G.: Spectral attenuation of global and diffuse UV irradiance and actinic flux by clouds, Q. J. Roy. Meteor. Soc., doi:10.1002/qj.2341, 2014.

McKenzie, R., Johnston, P., Hofzumahaus, A., Kraus, A., Madronich, S., Cantrell, C., Calvert, J., and Shetter, R.: Relationship between photolysis frequencies derived from spectroscopic measurements of actinic fluxes and irradiances during the IPMMI campaign, J. Geophys. Res.-Atmos., 107, ACH 1-1–ACH 1-16, doi:10.1029/2001JD000601, 2002.

McKenzie, R. L., Aucamp, P. J., Bais, A. F., Björn, L. O., Ilyas, M., and Madronich, S.: Ozone depletion and climate change: impacts on UV radiation, Photoch. Photobio. Sci., 10, 182–198, doi:10.1039/C0PP90034F, 2011.

Micheletti, M. I., Piacentini, R. D., and Madronich, S.: Sensitivity of biologically active UV radiation to stratospheric ozone changes: effects of action spectrum shape and wavelength range, Photochem. Photobiol., 78, 456–461, 2003.

Monks, P. S., Carpenter, L. J., Penkett, S. A., Ayers, G. P., Gillett, R. W., Galbally, I. E., and Meyer, C. P.: Fundamental ozone photochemistry in the remote marine boundary layer: the SOAPEX experiment, measurement and theory, Atmos. Environ., 32, 3647–3664, 1998.

Rohrer, F. and Berresheim, H.:Strong correlation between levels of tropospheric hydroxyl radicals and solar ultraviolet radiation, Nature, 442(7099):184–187, doi:10.1038/nature04924, 2006.

Sander, S. P., Friedl, R. R., Golden, D. M., Kurylo, M. J., Moortgat, G. K., Keller-Rudek, H., Wine, P. H., Ravishankara, A. R., Kolb, C. E., Molina, M. J., Finlayson-Pitts, B. J., Huie, R. E., and Orkin, V. L.: Chemical kinetics and photochemical data for use in atmospheric studies, Evaluation Number 15, JPL Publication 06-2, Jet Propulsion Laboratory, Pasadena, 2006.

Schade, N. H., Macke, A., Sandmann, H., and Stick, C.: Total and partial cloud amount detection during summer 2005 at Westerland (Sylt, Germany), Atmos. Chem. Phys., 9, 1143–1150, doi:10.5194/acp-9-1143-2009, 2009.

Schallhart, B., Huber, A., and Blumthaler, M.: Semi-empirical method for the conversion of spectral UV global irradiance data into actinic flux, Atmos. Environ., 38, 4341–4346, 2004.

Sommariva, R., Haggerstone, A.-L., Carpenter, L. J., Carslaw, N., Creasey, D. J., Heard, D. E., Lee, J. D., Lewis, A. C., Pilling, M. J., and Zádor, J.: OH and HO_2 chemistry in clean marine air during SOAPEX-2, Atmos. Chem. Phys., 4, 839–856, doi:10.5194/acp-4-839-2004, 2004.

Webb, A. R., Kift, R., Thiel, S., and Blumthaler, M.: An empirical method for the conversion of spectral UV irradiance measurements to actinic flux data, Atmos. Environ., 36, 4397–4404, 2002.

Wilson, S. R. and Forgan, B. W.: Aerosol optical depth at Cape Grim, Tasmania 1986–1999, J. Geophys. Res., 107, 4068, doi:10.1029/2001JD000398, 2002.

Wilson, S. R. and Shinkfield, P.: Passive Solar Radiation, in: Baseline Atmospheric Program 2005–2006, edited by: Cainey, J. M., Derek, N., and Krummel, P. B., Australian Bureau of Meteorology and CSIRO Marine and Atmospheric Research, Melbourne, p. 98, 2007.

Wilson, S. R.: The Cape Grim Scanning UV Spectrometer, in: Baseline Atmospheric Program 2003–2004, edited by: Cainey, J. M., Derek, N., and Krummel, P. B., Bureau of Meteorology/CSIRO Atmospheric Research, Melbourne, 9–16, 2006.

Wilson, S. R.: Effect of Temperature on the Cape Grim UV-B Records, in: Baseline Atmospheric Program 2005–2006, edited by: Cainey, J. M., Derek, N., and Krummel, P. B., Australian Bureau of Meteorology and CSIRO Marine and Atmospheric Research, Melbourne, 25–30, 2007.

Wilson, S. R. and Forgan, B. W.: In situ calibration technique for UV spectral radiometers, Appl. Optics, 34, 5475–5484, 1995.

Ylianttila, L. and Schreder, J.: Temperature effects of PTFE diffusers, Opt. Mater., 27, 1811–1814, doi:10.1016/j.optmat.2004.11.008, 2005.

Young, S. A.: Interpretation of the MiniLIDAR Data Recorded at Cape Grim 1998–2000, in: Baseline Atmospheric Program 2005–2006, edited by: Cainey, J. M., Derek, N., and Krummel, P. B. Australian Bureau of Meteorology and CSIRO Marine and Atmospheric Research, Melbourne, 15–24, 2007.

Table 1. Monthly mean photolysis rate $J(O^1D)$. This is calculated using hourly averages for each of the 24 h in the day.

Month	Mean (std. deviation) $s^{-1} \times 10^{-6}$
1	9.62 (0.54)
2	8.17 (0.60)
3	5.00 (0.59)
4	2.57 (0.25)
5	1.36 (0.20)
6	0.65 (0.05)
7	0.70 (0.03)
8	1.25 (0.08)
9	2.61 (0.55)
10	4.33 (0.59)
11	7.16 (0.37)
12	9.34 (0.56)

Table 2. Results for fitting $J(O^1D)$ with the form shown in Eq. (7). Brackets [...] surround values that have been assumed in the fit. Uncertainties (in brackets) are standard errors in the last quoted figure of the fitted parameters. Units for A_1 and A_2 are s^{-1}. The "median fit" is a fit to the medians as shown in Fig. 5.

Fit	$A_1/10^{-4}$	B_1	$A_2/10^{-5}$	B_2	RAF	R^2
All data	1.752(8)	1.743(3)			1.531(9)	0.859
	4.8(2)	3.07(5)	2.8(2)	0.91(2)	1.555(9)	0.865
Medians	2.3(2)	1.92(7)			[1.53]	0.996
	4.1(3)	2.7(1)	1.5(4)	0.69(9)	[1.53]	1.000
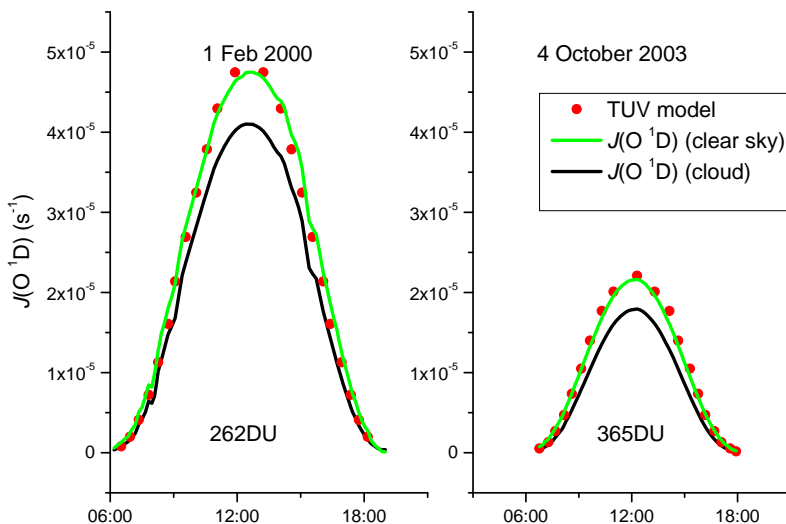
Figure 1. Comparison of clear sky calculation values to measurements. Calculations have been performed with the column ozone amount reported by the TOMS satellite. $J(O^1D)$ has been calculated using an α of 2.0 relevant to clear skies (green line) and 1.73 (cloudy - black line).
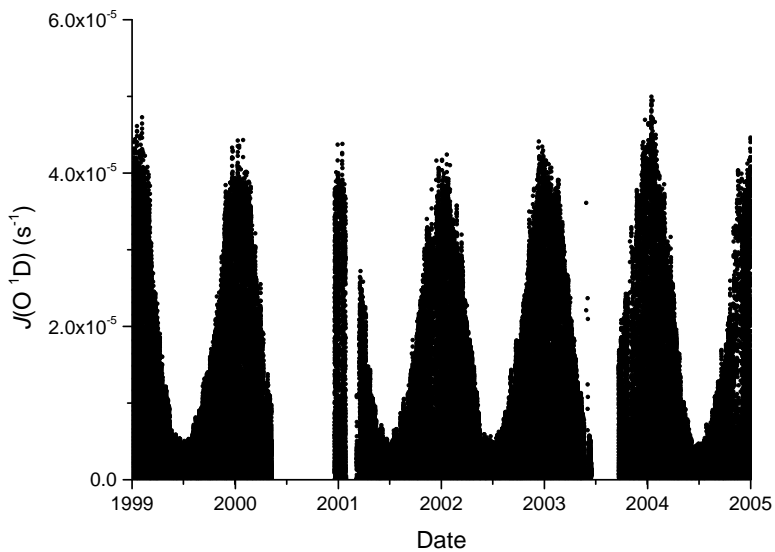
Figure 2. Photolysis rate $J(O^1D)$ observed at Cape Grim 2000–2005. Gaps in the data are due to instrument failure.
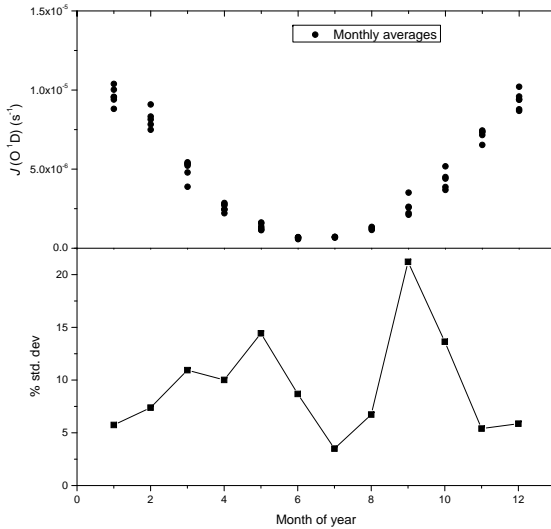
Figure 3. Annual cycle of $J(O^1D)$. The bottom panel shows the scatter in the monthly values as a percentage of the monthly mean.
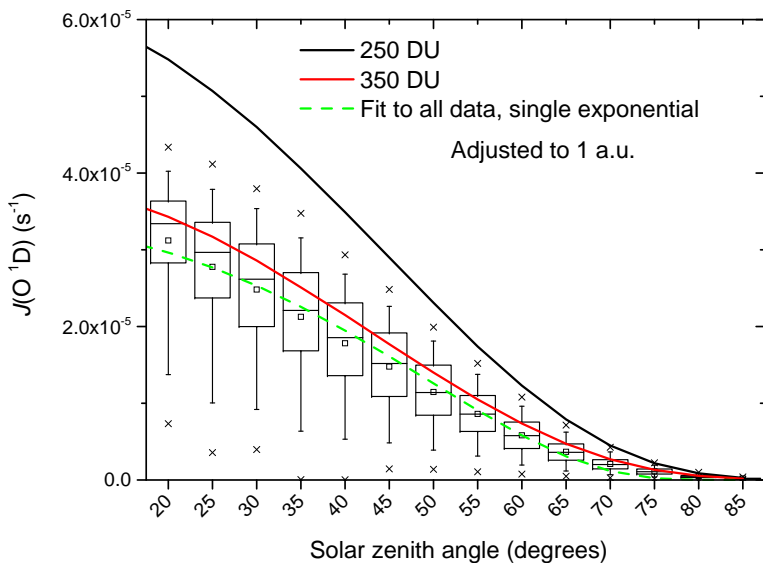
Figure 4. Solar zenith angle dependence of $J(O^1D)$. Crosses mark the 1 and 99 percentile. The boxes span $25/75\%$, the whiskers mark 10 and 90 %, the central line indicates the median and the square the average value. The x axis value is the central value of the $5°$ bin used. The two solid lines were calculated using TUV (V 5.0) for ozone column amounts of 250 DU (February) (black solid line) and 350 DU (September)(red solid line). The short-dashed green line is the fit to a single exponential term to all data.
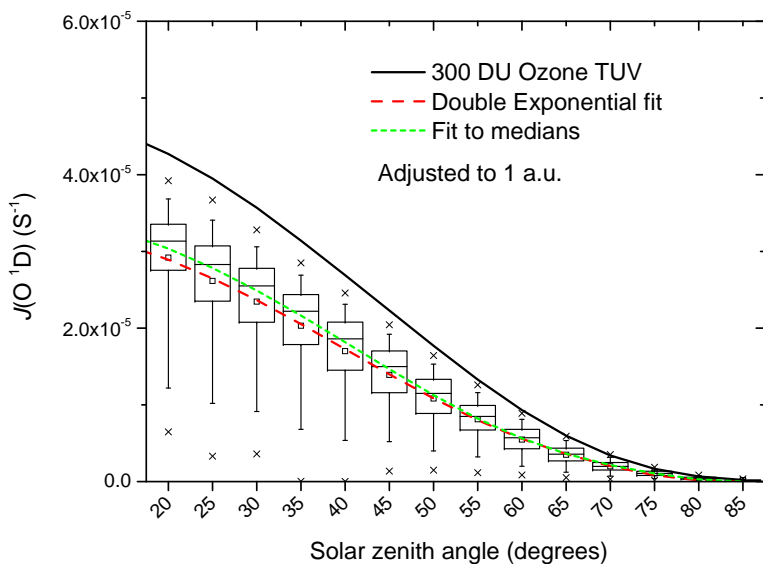
27

Figure 5. Cape Grim measurements of $J(O^1D)$ adjusted to a nominal 300 DU and 1 a.u.. The solid line is the calculated $J(O^1D)$ for clear skies and 300 DU ozone column and an aerosol optical depth of 0.05 using TUV 5.0 (Madronich and Flocke, 1997). The two broken lines are the results of the fits using two exponential terms to either all data or the median value of each bin (see also Table 2).
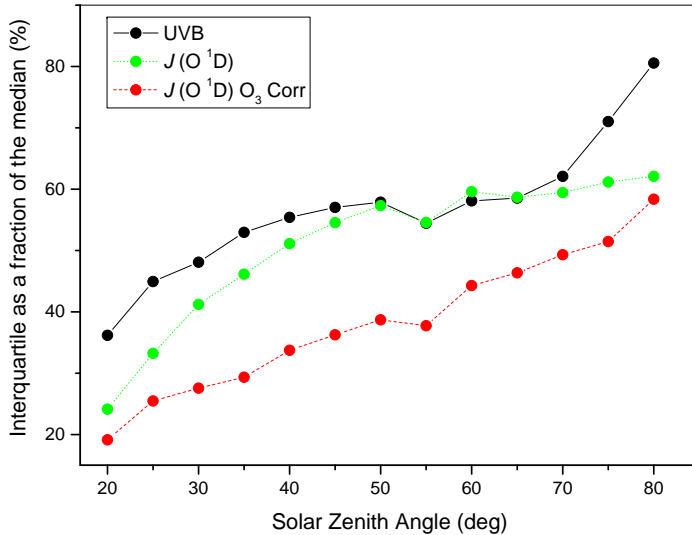
28

Figure 6. The interquartile (75–25 %) difference as a percentage of the median value as a function of solar zenith angle. UVB is the global irradiance, and the other two terms are the derived photolysis rates, with the red curve measurements have been corrected to a constant column ozone amount.
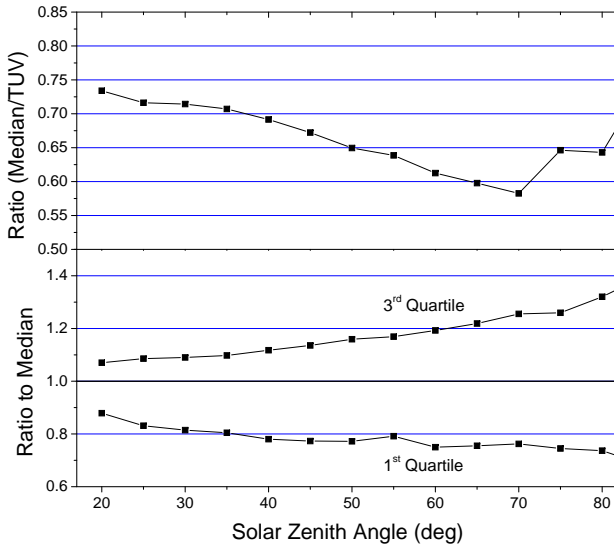
Figure 7. Top panel shows the ratio of the median measured $J(O^1D)$ to that from a calculation for clear skies. The bottom panel shows the spread in quartile values as a ratio to the median.